Acta Crystallographica Section D
Biological Crystallography
ISSN 0907-4449

Structure of *Escherichia coli* YhdH, a putative quinone oxidoreductase

Gerlind Sulzenbacher,[a] Véronique Roig-Zamboni,[a] Fabienne Pagot,[a] Sacha Grisel,[a] Aurelia Salomoni,[a] Christel Valencia,[a] Valérie Campanacci,[a] Renaud Vincentelli,[a] Mariella Tegoni,[a] Hans Eklund[b] and Christian Cambillau[a]*

[a]AFMB, UMR 6098, CNRS and Universités Aix-Marseille I and II, 31 Chemin J. Aiguier, F-13402 Marseille CEDEX 20, France, and [b]Department of Molecular Biology, SLU, BMC, Box 256, 751 05, Uppsala, Sweden

Correspondence e-mail: cambillau@afmb.cnrs-mrs.fr

Received 30 July 2004
Accepted 16 August 2004

PDB References: native YhdH, 1o89, r1o89sf; YhdH–NADP complex, 1o8c, r1o8csf.

As part of a structural genomics project on bacterial gene products of unknown function, the crystal structures of YhdH, a putative quinone oxidoreductase, and its complex with NADP have been determined at 2.25 and 2.6 Å resolution, respectively. The overall fold of YhdH is very similar to that of alcohol dehydrogenases and quinone reductases despite its low sequence identity. The absence of any Zn ion indicates that YdhH is a putative quinone oxidoreductase. YhdH forms a homodimer, with each subunit composed of two domains: a catalytic domain and a coenzyme-binding domain. NADP is bound in a deep cleft formed between the two domains. Large conformational changes occur upon NADP binding, with the two domains closing up to each other and narrowing the NADP-binding cleft. Comparisons of the YdhH active site with those of the quinone oxidoreductases from *Escherichia coli* and *Thermus thermophilus* made it possible to identify essential conserved residues as being Asn41, Asp43, Asp64 and Arg318. The active-site size is very narrow and unless an induced fit occurs is accessible only to reagents the size of benzoquinone.

1. Introduction

Structural genomics represents an excellent tool to provide the ultimate understanding of the function of each gene product by unravelling its three-dimensional structure. We have undertaken a medium-scale structural genomics project with the aim of elucidating the three-dimensional structures of 110 *Escherichia coli* targets of unknown function (Abergel *et al.*, 2003). These targets have been selected on the basis of high sequence homology with the gene products of a wide range of

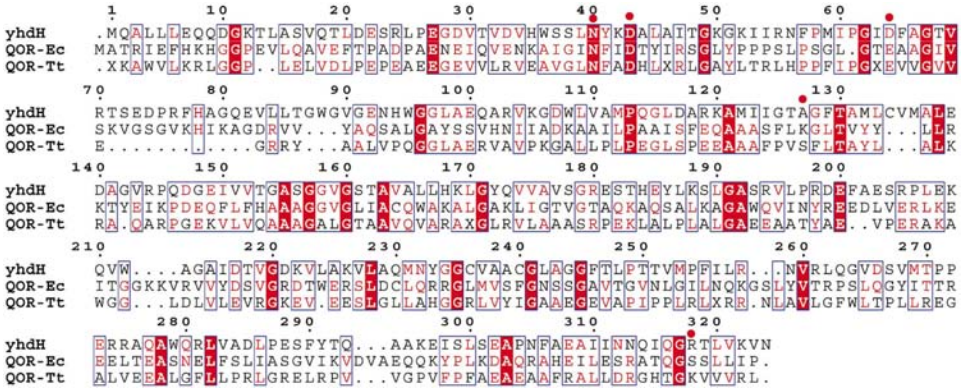

Figure 1
Sequence alignment of YhdH, *E. coli* QOR and *T. thermophilus* QOR. Numbering used is that of YhdH. Red filled boxes denote identical residues and blue circled boxes denote homologous residues. The putative catalytic residues are marked by a red circle (alignment performed with *MULTIALIGN*; Corpet, 1988).

Table 1
Data-collection and processing statistics for YhdH.

Values in parentheses are for the highest resolution shell.

	MAD			
	Peak (Se)	Remote (Se)	Native	NADP complex
Beamline	ESRF-ID29	ESRF-ID29	ESRF-EH1	ESRF-EH1
Wavelength	0.9796	0.9252	0.934	0.934
Space group	$P4_322$	$P4_322$	$P4_322$	$P6_1$
Unit-cell parameters				
$a = b$ (Å)	55.52	55.52	55.67	189.31
c (Å)	196.90	196.90	201.48	98.65
Molecules per AU	1	1	1	5
Resolution range	40–2.60 (2.74–2.60)	40–2.6 (2.74–2.60)	20–2.25 (2.31–2.25)	45–2.60 (2.67–2.60)
$R_{\rm merge}$†	0.083 (0.238)	0.078 (0.224)	0.049 (0.450)	0.050 (0.192)
$R_{\rm anom}$‡	0.071 (0.154)	0.054 (0.195)		
No. observations	41798	34341	426724	563701
No. unique reflections	10180	10144	15944	62012
Completeness (%)	99.9 (99.6)	99.6 (99.6)	99.1 (99.7)	100 (100)
Redundancy	4.1 (4.3)	3.4 (3.5)	8.6 (8.9)	6.1 (5.9)
$\langle I/\sigma(I)\rangle$	6.3 (3.0)	7.2 (2.9)	11.66 (1.8)	8.3 (3.9)
B from Wilson statistics	53.21	52.42	50.08	46.44

† $R_{\rm merge} = \sum_{hkl}\sum_i |I_{hkli} - \langle I_{hkli}\rangle|/\sum_{hkl}\sum_i \langle I_{hkli}\rangle$. ‡ $R_{\rm anom} = \sum |\langle I^+\rangle - \langle I^-\rangle|/\sum(\langle I^+\rangle + \langle I^-\rangle)$.

Table 2
Refinement and model statistics.

	Native	NADP complex
Resolution used in refinement (Å)	12–2.25	45–2.6
No. protein atoms†	2406	9752
No. water molecules/ligand atoms†	54/—	348/198
$R_{\rm cryst}$‡/ $R_{\rm free}$ (%)	19.70/23.67	18.93/21.25
R.m.s. 1–2 bond distances (Å)	0.011	0.005
R.m.s. 1–3 bond angles (°)	1.16	0.95
R.m.s. chiral volumes (Å^3)	0.068	0.066
Average main/side-chain B (Å^2)	62.94/66.99	47.13/50.45
Average B, solvent/ligand (Å^2)	55.87/—	36.02/45.23
Main-chain ΔB, bonded atoms (Å^2)	1.81	1.069
Ramachandran plot outliers	None	None

† Per asymmetric unit, corresponding to either one (native) or five (complex) molecules of YhdH. ‡ $R_{\rm cryst} = \sum \big||F_{\rm o}| - |F_{\rm c}|\big|/\sum |F_{\rm o}|$.

Table 3
Putative catalytic residues identified by sequence comparisons or by three-dimensional structure superposition in *E. coli* and *T. thermophilus* QORs and in YhdH (bold).

E. coli QOR (1qor)	*T. thermophilus* QOR (1iyz)	YhdH (1o8c)
Asn41	Asn38	Asn40
Lys124 NZ	**Lys297 NZ**	**Arg318 NH1**
Asp44 OD1	Asp41	Asp43
Glu64 OE1	Glu62 OE1	**Asp64 OD1**

Gram-negative and Gram-positive bacteria and an identity of less than 30% with any protein of known structure in order to discover new targets for the development of new antibiotics. Furthermore, low or no homology with eukaryotic ORFs was taken to be a favourable feature. When the target list of our programme was set up, a sequence-alignment search with the YhdH sequence using the BLAST submission server against the PDB returned no sequence similarity with any protein of known structure. A sequence-alignment search against the non-redundant database of sequences, NR, returned a putative function of quinone oxidoreductase. YhdH therefore fitted our requirements well.

YhdH presents sequence similarities to alcohol dehydrogenases (ADHs; Hempel *et al.*, 1993; Hurley *et al.*, 1997) and quinone oxidoreductases (QORs; Thorn *et al.*, 1995; Shimomura *et al.*, 2003), two members of the family of NAD(P)-dependent oxidoreductases. Its sequence identity with horse liver ADH (Eklund *et al.*, 1981) is 18%, while it is 16 and 25% with the QORs from *Escherichia coli* (Thorn *et al.*, 1995) and *Thermus thermophilus* (Shimomura *et al.*, 2003), respectively (Fig. 1). It would therefore be difficult to distinguish between an ADH or QOR function on the sole basis of sequence identity. However, the medium-chain NAD(P)-dependent oxidoreductase family is split into two subfamilies (Edwards *et al.*, 1996), one of which contains the ADHs, such as horse-liver ADH (Eklund *et al.*, 1981), and the other the QORs, such as *E. coli* QOR (Thorn *et al.*, 1995) and ζ-crystallin (Rodokanaki *et al.*, 1989), some members of which have been found in plants (Mano *et al.*, 2000, 2002). The main

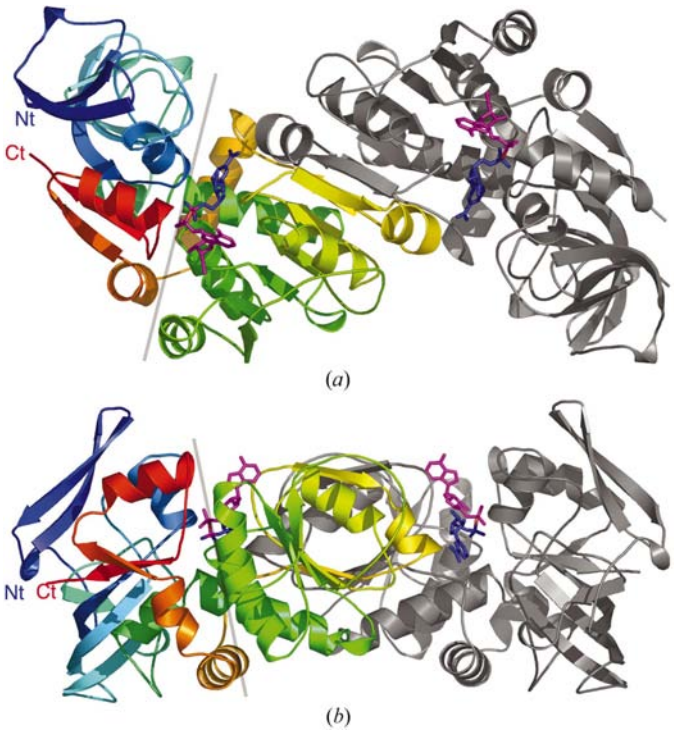

Figure 2
Ribbon view of the YhdH dimer. (*a*) The first monomer is in grey and the second in colour. The grey line delimits the two domains of each monomer. The NADP molecules are represented in stick representation; the nicotinamide moiety is coloured blue and the adenosine moiety coloured magenta. (*b*) The same view rotated by 90°. This figure was produced with *PyMol* (DeLano Scientific).

difference between the two subfamilies is that ADHs contain a catalytic Zn^{2+} ion and in many cases also a structural Zn^{2+} ion, while QORs are devoid of any cations. Noticeably, while the mechanism of ADHs has been subjected to a wealth of studies and is now well known, very little is known about QORs. Only two QOR structures have been described to date, compared with several tens of structures of ADHs. Recently, the structure of a quinone oxidoreductase from the thermophilic bacteria *T. thermophilus* and its complex with NADP have been described (Shimomura *et al.*, 2003). This enzyme presents sequence (Fig. 1) and structural homology with YhdH and the enzymes are most probably orthologues.

In this paper, we describe the three-dimensional structure of YhdH, solved using the MAD technique, in its native state and its binary complex with NADP at 2.6 Å resolution. Structural analysis of the narrow active site suggests that it might be a quinone oxidoreductase active towards monocyclic quinones such as benzoquinone.

2. Materials and methods

2.1. Cloning, expression and purification

The general strategy has been described elsewhere (Vincentelli *et al.*, 2003). DNA fragment ORF_o324 encoding YhdH was amplified from the genome of *E. coli* strain K-12 by PCR and subcloned into the Gateway system (Invitrogen, pDest17 plasmid), introducing 15 amino acids plus six histidines at the N-terminus (Walhout *et al.*, 2000). Expression was carried out using *E. coli* Tuner (DE3)pLys cells grown in LB medium at 310 K. Bacterial cells were lysed by treatment with lysozyme and consequent freeze-thawing. Nickel-ion affinity chromatography was performed on a Pharmacia Äkta FPLC with an IMAC column, followed by preparative gel filtration. Selenomethionine-substituted enzyme was produced using the same bacterial strain grown in minimal M9 medium and supplemented before induction with selenomethionine and amino acids known to inhibit methionine biosynthesis (Doublié, 1997). Purified protein was characterized by SDS–PAGE, MALDI–TOF mass spectroscopy, circular dichroism and dynamic light scattering (DLS). DLS analysis of the protein solution gave a polydispersity of approximately 15% of the particle radius and clearly indicated the dimeric state of the protein.

2.2. Crystallization and data collection

Sitting-drop vapour-diffusion crystallization screens were set up with a TECAN Genesis robot (Sulzenbacher *et al.*, 2002) on Greiner microtitre plates (Greiner 609160 or 609120, Friekenhausen, Germany). 1.5 µl droplets of protein solution at 27 mg ml^{-1} were tested against equal amounts of 244

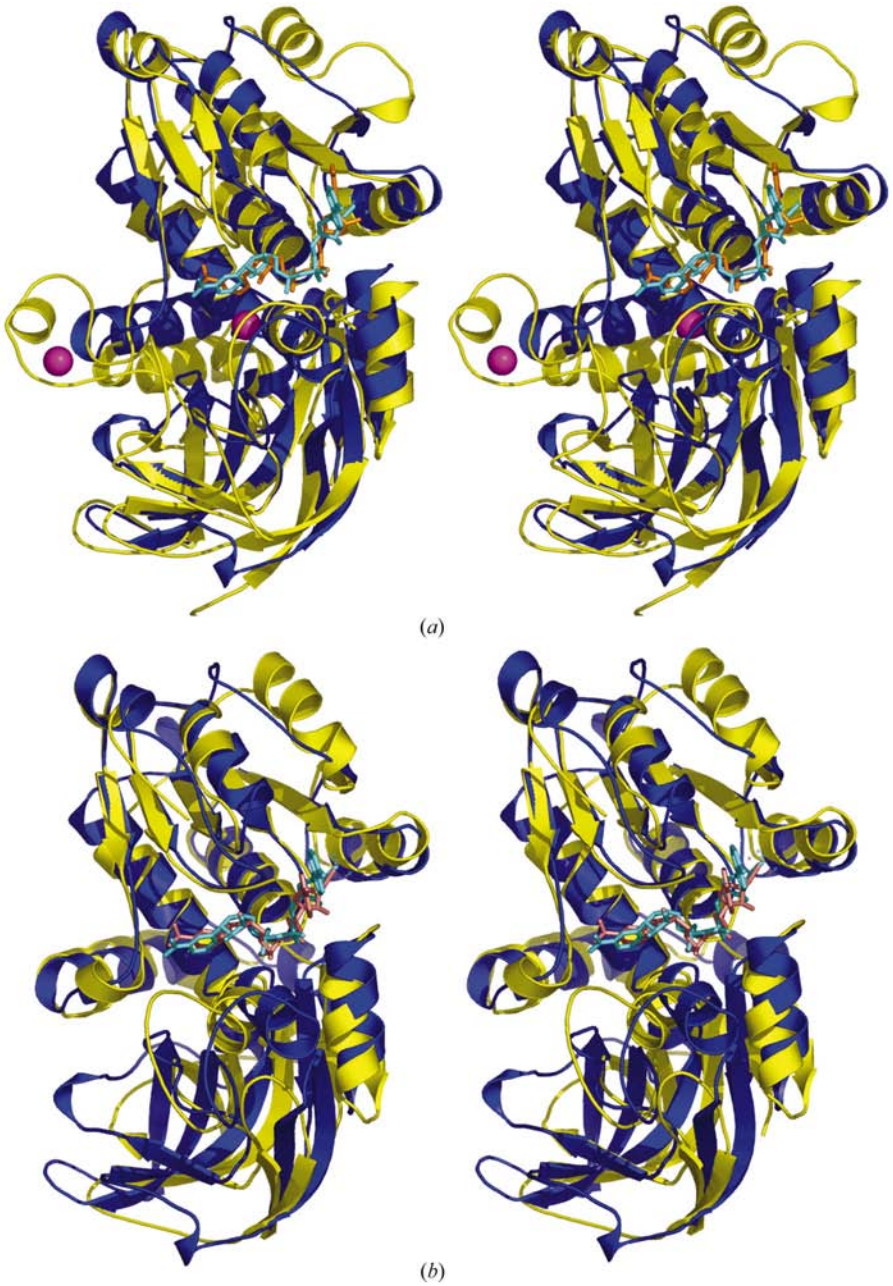

Figure 3
Stereo ribbon views of superposition of YhdH with related structures. (*a*) YhdH (blue) superimposed on horse liver ADH (yellow); Zn atoms are in magenta and and NADP is in orange. Note the horse liver ADH extra domain accommodating the structural Zn. (*b*) YhdH (blue) superimposed on *T. thermophilus* QOR (PDB code 1iyz; yellow; NADP in fuschia). The figure was produced with *PyMol*.

crystallization conditions provided by commercial kits: Stura Footprint Screen (Stura *et al.*, 1992), Wizard Screens I and II (Emerald BioStructures, http://www.emeraldbiostructures.com) and Structure Screens 1 and 2 (Jancarik *et al.*, 1991). A first hit appeared with condition II D1 of Stura Footprint Screen (42% PEG 600, 0.2 *M* imidazole–malate pH 5.5) and was further refined by traditional methods employing the hanging-drop vapour-diffusion method in Linbro plates. Final crystallization conditions for both the native and the selenomethionine-substituted protein consisted of 39% PEG 600, 0.1 *M* HEPES pH 7.5. Crystals of the YhdH–NADP complex were obtained by incubating YhdH at 6 mg ml^{-1} overnight with 5 m*M* NADP and 0.1 m*M* $ZnCl_2$ and following the same general procedure adopted for crystallization of the native protein. Final crystallization conditions for the complex consisted of 8.5% PEG 8K, 0.1 *M* sodium acetate pH 5.5 and 0.01 m*M* $ZnCl_2$. Crystals of the native and the selenomethione-substituted protein belong to space group $P4_322$ and contain one molecule per asymmetric unit, whereas crystals of the YhdH–NADP complex belong to space group $P6_1$ and contain five molecules per asymmetric unit. All data sets were collected at 100 K from flash-frozen crystals. Cryosolutions were of the same composition as the crystallization solutions but supplemented with 30% PEG 400.

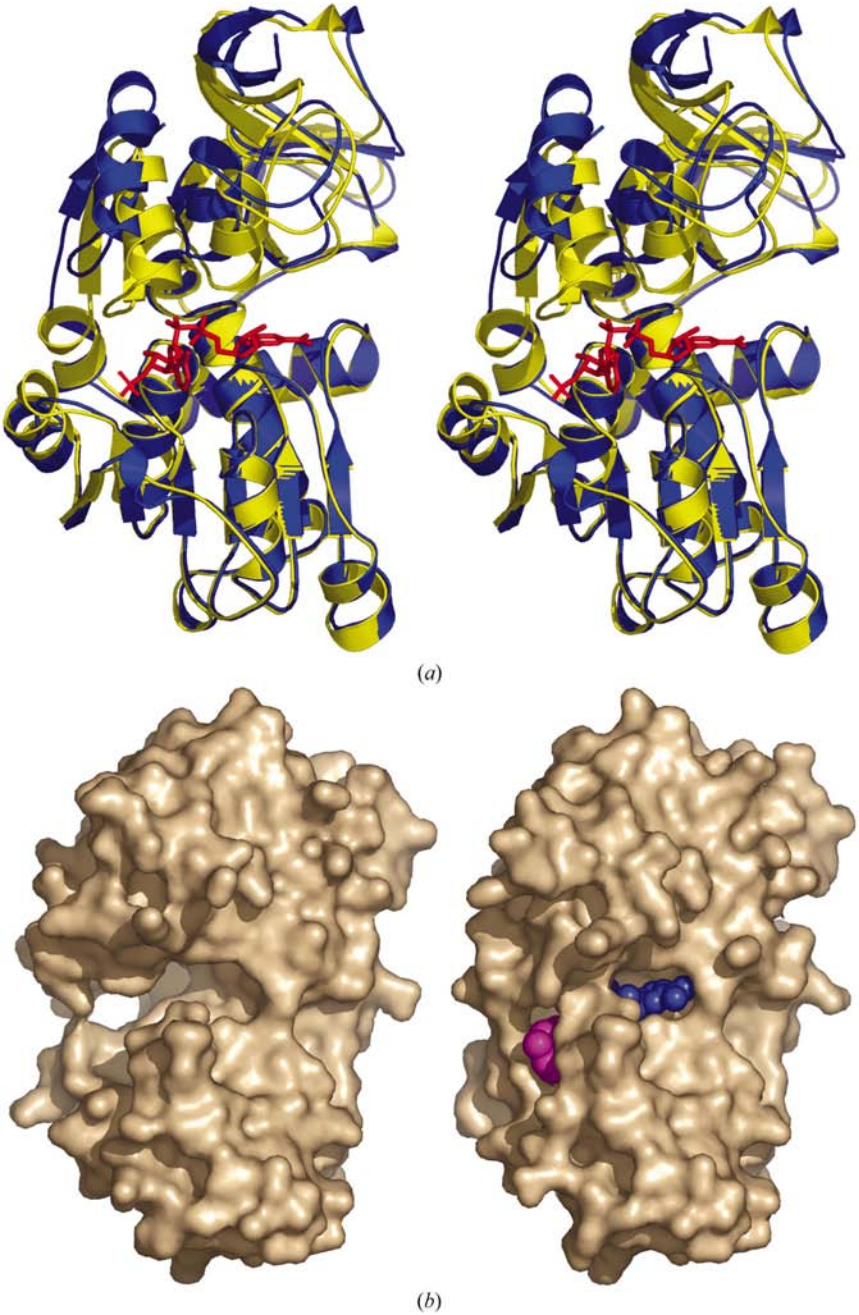

Figure 4
Views resulting from the superposition of the Rossmann-fold domains of apo and holo YhdH. (*a*) Stereo ribbon view of apo YhdH (blue) superimposed on holo YhdH (yellow; NADP in red). (*b*) Molecular surface of apo YhdH (left) and holo YhdH (right). Note the closure of the monomer obtained by rotation of each domain towards the other, which results in a tight binding of NADP (the nicotinamide moiety is coloured blue and the adenosine moiety is coloured magenta). The figure was produced with *PyMol*.

A two-wavelength MAD data set for selenomethionine-substituted YdhD was collected on beamline ID29 (ESRF, Grenoble) and data sets for native YhdH and for the YhdH–NADP complex were collected on beamline ID14-EH1 (ESRF, Grenoble). Data were indexed and integrated with *DENZO* (Otwinowski & Minor, 1997) and all further computations carried out with the *CCP*4 program suite (Collaborative Computational Project, Number 4, 1994), unless otherwise stated. Data-collection statistics are summarized in Tables 1 and 2.

2.3. Structure resolution and refinement

The structure of YhdH was solved using the program *SOLVE* (Terwilliger & Berendzen, 1999*b*). The initial MAD phases had a mean figure of merit of 0.40 for data to 2.8 Å resolution and of 0.61 after density modification with the program *RESOLVE* (Terwilliger & Berendzen, 1999*a*). The experimental electron-density map was of good quality and an almost continuous protein chain was manually traced and fitted with the program *TURBO-FRODO* (Roussel & Cambillau, 1991). The resulting model was refined against the native data set, extending to higher resolution. Rigid-body refinement and simulated annealing were carried out with the program *CNS* (Brünger *et al.*, 1998) and the model was further refined with the program *REFMAC* (Murshudov *et al.*, 1997), using the maximum-likelihood method and incorpor-

ating bulk-solvent corrections, anisotropic F_{obs} *versus* F_{calc} scaling and TLS refinement. A random 10% (1550) of reflections were set aside for cross-validation purposes. Automated solvent building was performed with the program *ARP*/*wARP* (Perrakis *et al.*, 1999). The final model was used as a template for the structure solution of the YhdH–NADP complex by molecular replacement using the program *MOLREP* (Vagin & Teplyakov, 1998). The complex structure was refined with the program *REFMAC* (Murshudov *et al.*, 1997) in the same fashion as the native structure, with the additional incorporation of NCS restraints. A random 5% (3140) of reflections were set aside for cross-validation purposes. Although clear difference electron density corresponding to bound NADP appeared from the beginning, the coordinates for the ligand were incorporated only towards the end of the refinement.

The stereochemistry of the final models was verified with the program *PROCHECK* (Laskowski *et al.*, 1993). Refinement and structure-quality statistics are listed in Table 3. Figures were generated with *PyMOL* (DeLano Scientific) and *TURBO-FRODO* (Roussel & Cambillau, 1991).

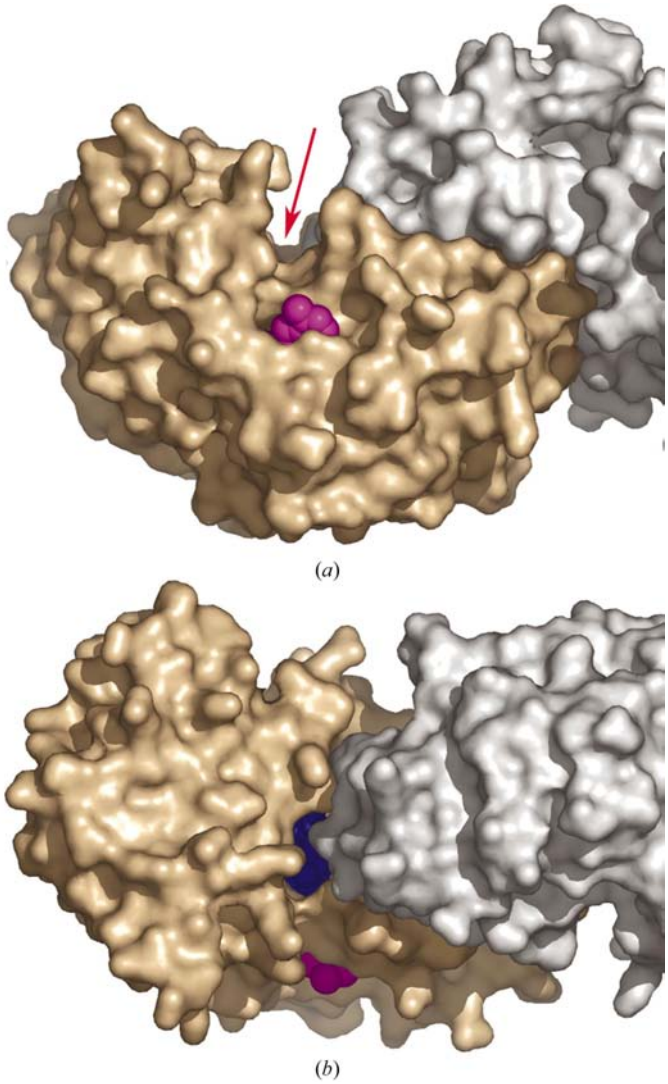

Figure 5
Molecular-surface representation of the active-site crevice entry. One monomer is coloured grey and the other light brown. Views (*a*) and (*b*) are rotated 90° around a horizontal axis. The NADP nicotinamide moiety is coloured blue and the adenosine moiety is coloured magenta. Note that the active-site crevice is made up of both subunits. The figure was produced with *PyMol*.

3. Results and discussion

3.1. Overall structure and putative function

The apo-YhdH structure contains a complete monomer chain of 324 residues in the asymmetric unit. A biological dimer can be readily reconstituted from a symmetry-related monomer. The asymmetric unit of holo-YhdH contains five monomers (2.5 dimers) of 324 amino acids and one NADP arranged in two biological dimers and a single monomer which can be associated with a symmetry-related monomer to form a biological dimer.

Each monomer is composed of two domains: a Rossmann fold, binding the NADP cofactor, and a catalytic domain (Fig. 2*a*). The dimer is assembled through a large interface, locked by two antiparallel strand–strand interactions: one involving the large β-sheets of both Rossmann-fold domains, the second involving two single β-strands (Fig. 2*b*, top).

Screening the PDB using the DALI server (Holm & Sander, 1995) with a holo-YhdH monomer returned five structures with r.m.s.d. values of between 2.4 and 2.9 Å: alcohol dehydrogenases (ADH) from *Pseudomonas aeruginosa* (PDB code 1llu; 2.4 Å; Levin *et al.*, 2004) and from horse liver (1hld; 2.7 Å; Eklund *et al.*, 1981), as well as an *E. coli* quinone oxidoreductase (1qor; 2.8 Å; Thorn *et al.*, 1995), a formaldehyde dehydrogenase (1kol; 2.8 Å; Tanaka *et al.*, 2002) and a ketose reductase (1e3j; 2.9 Å; Banfield *et al.*, 2001). In addition, the recently solved structure of the holo QOR from *T. thermophilus* (PDB code 1iyz; Thorn *et al.*, 1995), not returned by DALI, could be superimposed with an r.m.s.d. value of 2.5 Å. Superposition of the structures of horse liver ADH (Fig. 3*a*) and QOR from *T. thermophilus* onto YhdH confirms the data provided by DALI (Fig. 3*b*).

Therefore, neither sequences nor structures indicate clearly whether YhdH is an ADH or a QOR. The structures of both the apo- and holoenzymes are, however, depleted of any ions. The small subdomain of horse liver ADH, bearing cysteines 97, 100, 103 and 111 which bind the structural Zn^{2+} ion, is absent in YhdH (Fig. 3*a*). Similarly, the residues binding the catalytic Zn^{2+} ion, two cysteines and an histidine, are replaced by Asn40, Ile63 and Thr153 in YhdH (Fig. 1*b*). Two cysteines close to each other (4.1 Å) are located near the nicotinamide ring of YhdH, suggesting that they might be an alternative binding site for Zn^{2+}, together with a still unidentified third partner. However, no sign of a metal is observed in the electron-density maps and these residues are located far from the active-site crevice in a crowded environment on the *B* face of the nicotinamide ring and not on the *A* face as in all other members of the family. Their involvement in Zn^{2+} binding is

therefore not likely and YhdH is thus most probably a quinone oxidoreductase.

3.2. Comparison between the apo- and holoenzymes

As in other members of the family, NADP binding occurs in an extended groove between the two domains of each monomer. Upon binding, the two domains rotate by 18° around the hinge residues Thr126 and Leu286 towards the NADP (Fig. 4*a*), narrowing the internal channel and restraining the access of water (Fig. 4*b*). Both the nicotinamide and the adenine moieties are visible at the two ends of the channel. The NADP-binding site involves numerous interactions comparable to those found in other members of the family mentioned above. The nicotinamide moiety interacts with segments 126–133, 239–243 and 265–268. Its amide group establishes two strong hydrogen bonds with the backbones of Ile256 (NH2 to O═C, distance 2.75 Å) and Ser267 (C═O to H—N, distance 2.6 Å). Apart from these interactions, all other contacts are non-bonding, including those of the ribose moiety.

3.3. The active site

The active site is located at the bottom of a canyon 12 Å deep formed by the wall of the two monomers (Fig. 5). The subunit that binds NADP forms a wall and the bottom of the canyon, while the other subunit forms the opposite wall (Fig. 5*b*). The crevice mouth is very narrow, formed of residues that are on average more mobile than the rest of the protein. This

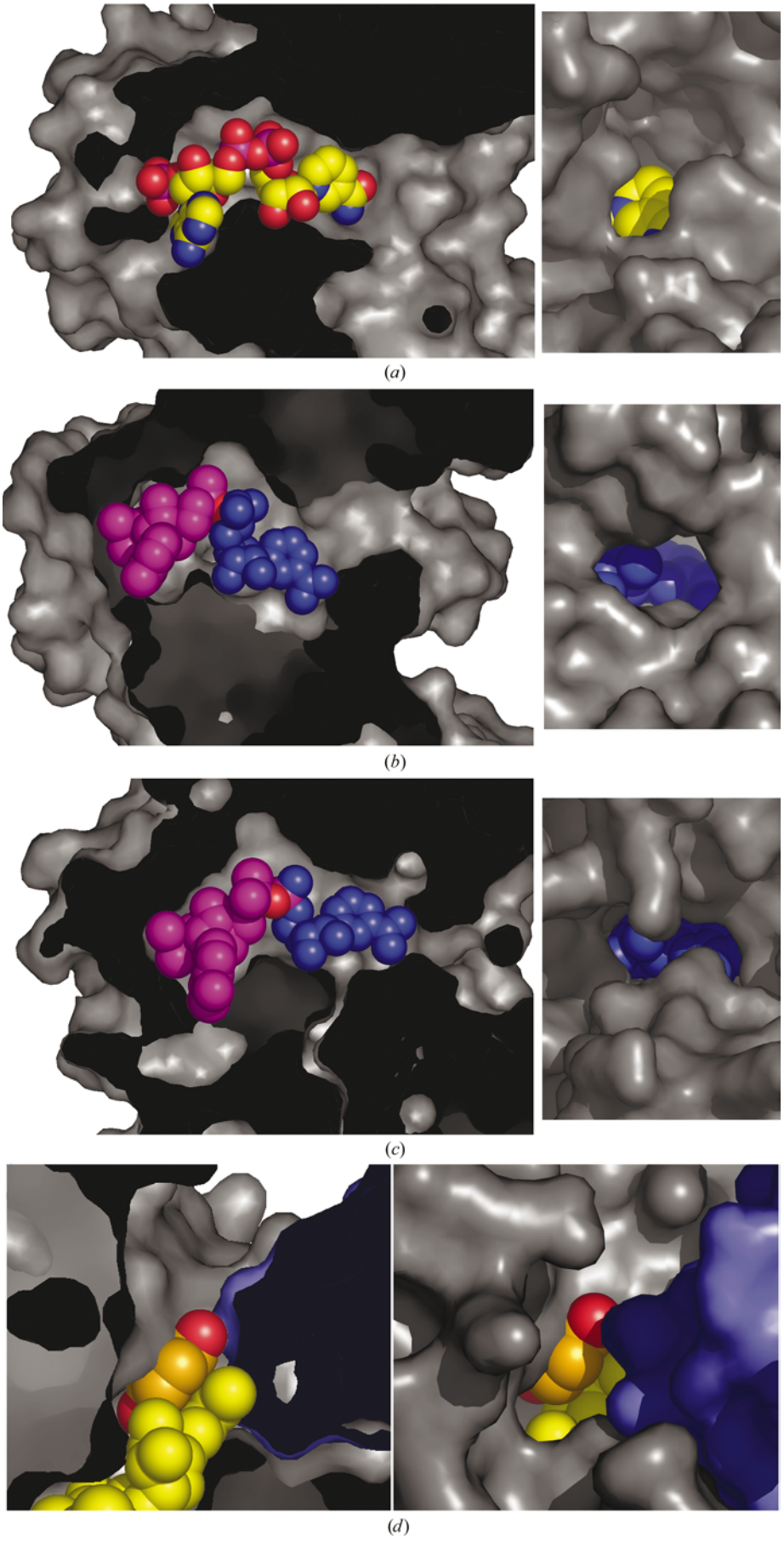

Figure 6
Molecular-surface representation of the extended active site (NADP- and quinone-binding site) of *E. coli* QOR (*a*), *T. thermophilus* QOR (*b*) and YhdH (*c*). The molecular surface has been slabbed at the level of NADP on the left, while the binding site is viewed from outside on the right. Note the reduction in the size of the binding site betwen *E. coli* QOR on one hand and *T. thermophilus* QOR and YhdH on the other. (*d*) Computer model of the benzoquinone binding in YhdH; slabbed view (left), front view (right). The figure was produced with *PyMol*.

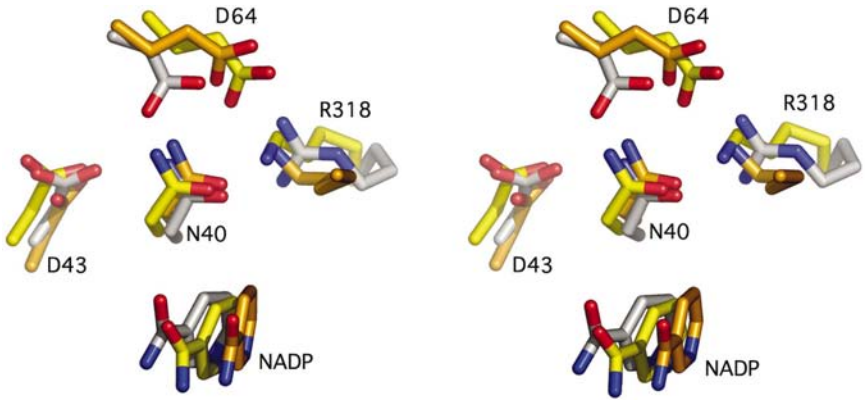

Figure 7
Stereoview of the superposition of conserved active-site residues of *E. coli* QOR (yellow C atoms), *T. thermophilus* QOR (orange C atoms) and YhdH (grey C atoms); O and N atoms are red and blue, respectively. Residues numbering is from YhdH. The figure was produced with *PyMol*.

includes Leu257(B) and Asp266 above the nicotinamide ring and Asn40, Lys42, Ile63, Glu92, Thr126, Thr130, Ser267 and Val286 opposite the NADP nicotinamide with regards to the cavity.

The structural differences in the substrate-binding sites of *T. thermophilus* QOR, *E. coli* QOR and YhdH may provide some insight into the physiological substrate of YhdH. Cutting a slice in the three structures at the level of the NADP channel makes it possible to compare the respective sizes of the three active-site crevices (Fig. 6). The crevice of *E. coli* QOR is very wide, since this enzyme can reduce large multi-ring substrates such as 5-hydroxy-1,4-naphthoquinone and phenanthraquinone (Thorn *et al.*, 1995). In contrast, *T. thermophilus* QOR has a narrower access for the substrate to NADP (Shimomura *et al.*, 2003) (Fig. 6*b*). Accordingly, *T. thermophilus* QOR cannot reduce multi-ring compounds and only has a reduction activity towards smaller compounds such as *p*-benzoquinone. YhdH has an even narrower channel access (Fig. 6*c*), barely the size of a single-ring quinonic compound. However, a benzoquinone could readily be modelled in the active site (Fig. 6*d*). One quinone oxygen can establish a strong hydrogen bond with the Lys42 amino group, while the second hydrogen can establish a hydrogen bond with Thr126 upon 120° side-chain rotation. The quinone ring stacks against the nicotinamide ring (with an ∼3 Å translation) at a distance of 3.1 Å. It should be noticed that without active-site rearrangement, compounds larger than benzoquinone cannot be accommodated.

3.4. The essential active site residues

Based on sequence and structure comparison between YhdH and the two QORs, essential active-site residues can be identified close to NADP, located on its *A* face (Table 3). Two residues are conserved in the three sequences: Asn40 and Asp43 (YhdH numbering; Fig. 5). Two other residues, Asp64 and Arg318, are not conserved. Asp64 is replaced by glutamic acids in the sequences of the *E. coli* and *T. thermophilus* QORs. However, the positions of the O atoms are superimposable (Fig. 7). Arg318 corresponds to a lysine in *T. thermophilus* QOR, but to a serine in *E. coli* QOR. The three-dimensional structure indicates, however, that *E. coli* QOR Lys124 is topologically equivalent: the NZ atoms of the two lysines and of the arginine superimpose well in the three-dimensional structures (Fig. 7). It can therefore be proposed that a common catalytic mechanism may exist based on the active groups whose topology is conserved.

4. Concluding remarks

The active site of YhdH resembles that of *T. thermophilus* QOR, indicating that it might be an *E. coli* QOR with narrower specificity. Interestingly, while the shape and size of the cavity seems to determine the substrate preference, a set of residues are conserved, indicating their possible involvement in catalysis. More than 20 bacterial sequences with 45–95% identity were identified in the NR database. This suggests that the function performed by YhdH should be conserved among numerous bacterial orthologues. Preliminary activity measurements of YhdH with several quinones (including benzoquinone) failed to reveal any measurable activity, indicating that the YhdH substrate might not be trivial to identify. This natural substrate deciphering is under way.

The ESRF is greatly acknowledged for beam time allocation. We thank the structural genomics team of the Marseille laboratory for technical assistance. This study was supported by the French Ministry of Industry (grant ASG) and is a collaboration with the IGS Laboratory and the Aventis company. This study was also supported by Marseille-Nice Genopole.

References

Abergel, C., Coutard, B., Byrne, D., Chenivesse, S., Claude, J. B., Deregnaucourt, C., Fricaux, T., Gianesini-Boutreux, C., Jeudy, S., Lebrun, R., Maza, C., Notredame, C., Poirot, O., Suhre, K., Varagnol, M. & Claverie, J. M. (2003). *J. Struct. Funct. Genom.* **4**, 141–157.
Banfield, M. J., Salvucci, M. E., Baker, E. N. & Smith, C. A. (2001). *J. Mol. Biol.* **306**, 239–250.
Brünger, A. T., Adams, P. D., Clore, G. M., DeLano, W. L., Gros, P., Grosse-Kunstleve, R. W., Jiang, J.-S., Kuszewski, J., Nilges, M., Pannu, N. S., Read, R. J., Rice, L. M., Simonson, T. & Warren, G. L. (1998). *Acta Cryst.* D**54**, 905–921.
Collaborative Computational Project, Number 4 (1994). *Acta Cryst.* D**50**, 760–763.
Corpet, F. (1988). *Nucleic Acids Res.* **16**, 10881–10890.
Doublié, S. (1997). *Methods Enzymol.* **276**, 523–530.
Edwards, K. J., Barton, J. D., Rossjohn, J., Thorn, J. M., Taylor, G. L. & Ollis, D. L. (1996). *Arch. Biochem. Biophys.* **328**, 173–183.
Eklund, H., Samma, J. P., Wallen, L., Branden, C. I., Akeson, A. & Jones, T. A. (1981). *J. Mol. Biol.* **146**, 561–587.
Hempel, J., Nicholas, H. & Lindahl, R. (1993). *Protein Sci.* **2**, 1890–1900.

Holm, L. & Sander, C. (1995). *Trends Biochem. Sci.* **20**, 478–480.
Hurley, T. D., Steinmetz, C. G., Xie, P. & Yang, Z. N. (1997). *Adv. Exp. Med. Biol.* **414**, 291–302.
Jancarik, J., Scott, W. G., Milligan, D. L., Koshland, D. E. Jr & Kim, S.-H. (1991). *J. Mol. Biol.* **221**, 31–34.
Laskowski, R., MacArthur, M., Moss, D. & Thornton, J. (1993). *J. Appl. Cryst.* **26**, 91–97.
Levin, I., Meiri, G., Peretz, M., Burstein, Y. & Frolow, F. (2004). *Protein Sci.* **13**, 1547–1556.
Mano, J., Babiychuk, E., Belles-Boix, E., Hiratake, J., Kimura, A., Inze, D., Kushnir, S. & Asada, K. (2000). *Eur. J. Biochem.* **267**, 3661–3671.
Mano, J., Torii, Y., Hayashi, S., Takimoto, K., Matsui, K., Nakamura, K., Inze, D., Babiychuk, E., Kushnir, S. & Asada, K. (2002). *Plant Cell. Physiol.* **43**, 1445–1455.
Murshudov, G., Vagin, A. A. & Dodson, E. J. (1997). *Acta Cryst.* D**53**, 240–255.
Otwinowski, Z. & Minor, W. (1997). *Methods Enzymol.* **276**, 307–326.
Perrakis, A., Morris, R. & Lamzin, V. S. (1999). *Nature Struct. Biol.* **6**, 458–463.
Rodokanaki, A., Holmes, R. K. & Borras, T. (1989). *Gene*, **78**, 215–224.
Roussel, A. & Cambillau, C. (1991). *Silicon Graphics Geometry Partners Directory*, p. 81. Mountain View, USA: Silicon Graphics.
Shimomura, Y., Kakuta, Y. & Fukuyama, K. (2003). *J. Bacteriol.* **185**, 4211–4218.
Stura, E. A., Matsumura, M., Fremont, D. H., Saito, Y., Peterson, P. A. & Wilson, I. A. (1992). *J. Mol. Biol.* **228**, 975–982.
Sulzenbacher, G. *et al.* (2002). *Acta Cryst.* D**58**, 2109–2115.
Tanaka, N., Kusakabe, Y., Ito, K., Yoshimoto, T. & Nakamura, K. T. (2002). *J. Mol. Biol.* **324**, 519–533.
Terwilliger, T. C. & Berendzen, J. (1999*a*). *Acta Cryst.* D**55**, 849–861.
Terwilliger, T. C. & Berendzen, J. (1999*b*). *Acta Cryst.* D**55**, 1872–1877.
Thorn, J. M., Barton, J. D., Dixon, N. E., Ollis, D. L. & Edwards, K. J. (1995). *J. Mol. Biol.* **249**, 785–799.
Vagin, A. & Teplyakov, A. (1998). *Acta Cryst.* D**54**, 400–402.
Vincentelli, R., Bignon, C., Gruez, A., Canaan, S., Sulzenbacher, G., Tegoni, M., Campanacci, V. & Cambillau, C. (2003). *Acc. Chem. Res.* **36**, 165–172.
Walhout, A. J., Temple, G. F., Brasch, M. A., Hartley, J. L., Lorson, M. A., van den Heuvel, S. & Vidal, M. (2000). *Methods Enzymol.* **328**, 575–592.